Contents lists available at ScienceDirect

Applied Catalysis B: Environmental

TiO$_2$/Al(H$_2$PO4)$_3$ composite film as separation-free and washing-resistance photocatalyst

Wenjun Jiang [a], Zhibao Qiu [b], Wenqing Yao [a,*], Yongfa Zhu [a], Wenquan Cui [b]

[a] Department of Chemistry, Tsinghua University, Beijing 100084, PR China
[b] College of Chemical Engineering, North China University of Science and Technology, Tangshan, Hebei 063009, PR China

ARTICLE INFO

ABSTRACT

Herein, TiO$_2$/Al(H$_2$PO4)$_3$ composite film was synthesized via a spray method. The composite film exhibited higher photocatalytic activity compared with pure TiO$_2$ (about 1.4-fold). TiO$_2$ nanoparticles were fixed on the framework of Al(H$_2$PO4)$_3$, which could prevent the agglomeration of TiO$_2$ nanoparticles and increase the reactive sites. More than that, the composite film was separation-free and bears good washing resistance thanks to the good adhesive force of Al(H$_2$PO4)$_3$. The good adhesive force could be ascribed to the formation of Ti—O—P bond between TiO$_2$ and Al(H$_2$PO4)$_3$, which also contributed to the increased photocatalytic activity. This work presents a feasible method of fabricating TiO$_2$-based separation-free and washing-resistance film, which may hold potential applications in the field of self-clean.

1. Introduction

Nano-photocatalysis technique has been considered one of the most promising techniques in the field of environmental remediation [1–3]. Although all kinds of photocatalysts, such as bismuth-based materials [4–8], cadmium-based materials [9–12], polymeric photocatalysts [13–15], have been developed, TiO$_2$ is still the most promising material in the field of practical pollutant treatment since TiO$_2$ holds the advantages of high stability, low-cost, environment-friendly and non-selective degradation towards various organic pollutants [11,16–22]. However, there are also some problems restricting its application range. Since most of the prepared TiO$_2$ is of nanometer size, the separation of TiO$_2$ from water is pretty difficult [13]. The frequently-used centrifugation method spends enormous amounts of energy, which is not economically feasible. As we all know, TiO$_2$ has super-hydrophilicity under UV light. So, the TiO$_2$ nanoparticles are easy to break off and be washed away when used as self-cleaning film, which seriously hinders the practical application of TiO$_2$. Hence, new ideas should be presented to address these issues.

Until now, lots of efforts have been made by researchers to address the separation and water erosion problems, such as magnetically separable photocatalysts [23,24], fibrous membrane photocatalysts via an electrospinning method [25] and 3D hydrogel photocatalysts [13,16], among which constructing TiO$_2$ film was regarded as the most facile method. The methods to construct TiO$_2$ film include liquid phase deposition [26], chemical vapor deposition [27,28], electrochemical deposition [29], sol-gel method [30,31] and magnetron sputtering [32]. However, the above-mentioned methods need high-level equipment and complex process.

Herein, we presented a spray method to construct TiO$_2$/Al(H$_2$PO4)$_3$ composite film as separation-free and washing-resistance photocatalyst. Al(H$_2$PO4)$_3$ is a kind of phosphate bonder and has the advantages of poisonless and tasteless, low cost, high adhesive property and room-temperature curable, which is widely used in the field of paint [33]. Al(H$_2$PO4)$_3$ could react with the substrate and form a stable composite structure by chemical bonds, making the composite film separation-free and with good washing resistance. In addition, TiO$_2$ nanoparticles was fixed on the framework of Al(H$_2$PO4)$_3$, which could prevent the agglomeration of TiO$_2$, increase the reactive sites and promote the photocatalytic performance.

2. Experimental section

2.1. Fabrication of TiO$_2$/Al(H$_2$PO4)$_3$ film

TiO$_2$ (P25, analytical pure grade) was obtained from Degussa. Al(H$_2$PO4)$_3$ was purchased from Shijiazhuang Xinsheng

---

* Corresponding author.
E-mail address: yaowq@mail.tsinghua.edu.cn (W. Yao).

Chemical Industrial Co. Ltd. All other reagents used were analytical pure and used without further purification. 0.8 g TiO_2 was dispersed in 100 mL DI water and stirred completely about 30 min to make a slurry. Then 0.02 g $Al(H_2PO_4)_3$ was added into the slurry and stirred completely about 12 h. Then the precursor solution was obtained (TiO_2 8 g/L, $Al(H_2PO_4)_3$ 0.2 g/L) and labelled as 0.2 g/L. According to the above method, a series of precursor solutions were obtained, labelled as 0 g/L (pure TiO_2 film), 0.4 g/L, 0.6 g/L, 0.8 g/L and 1.0 g/L. Then the above precursor solution was sprayed onto glass slide (2.5 cm × 3.5 cm) for two times using a high-pressure spray gun (NEW71-1.8S). At last, let the composite film air-dry and then dried at 60 °C for 30 min. Similarly, the precursor solution could also be sprayed onto wire mesh (4 cm × 6 cm) for three times.

2.2. Characterization

The morphology of the samples was observed by a Hitachi HT-7700 TEM, Hitachi SU-8010 FESEM and JEM 2100F HRTEM. X-ray diffraction (XRD) patterns of the samples were characterized by a Bruker D8 Advance X-ray diffractometer. The diffuse reflectance absorption spectra (DRS) of the samples was recorded on a UV–vis spectrophotometer (Hitachi UV-3900). The BET specific surface area of the samples was carried out by nitrogen adsorption using a Micromeritics 3020 instrument. X-ray photoelectron spectroscopy (XPS) examination was recorded using a PHI Quantera SXMTM system. Raman spectra were carried out on a HORIBA HR800 Raman spectrometer (514.5 nm).

2.3. Evaluation of photocatalytic performance

The photocatalytic activities of $TiO_2/Al(H_2PO_4)_3$ composite films were evaluated via the photocatalytic oxidation of methylene blue (MB) in solution under UV light irradiation. 12 W mercury lamp ($\lambda = 254$ nm) was adopted to get UV light. A home-made quartz cells (4.5 cm × 4.5 cm × 6.0 cm, shown in Fig. S1) were used as reactor. In a typical reaction: $TiO_2/Al(H_2PO_4)_3$ composite film was fixed in the reactor and 100 mL, 0.01 mM MB aqueous solution was added into the reactor. Before irradiation, the MB aqueous solution was magnetically stirred in dark for 30 min to achieve an absorption-desorption equilibrium between the film and MB. At given time intervals, 3 mL aliquots were sampled and analyzed by recording the absorbance at the characteristic band of 664 nm using a Hitachi U-3900 UV–vis spectrophotometer. For pure TiO_2 film, the solution should be centrifuged to remove some little particles, since TiO_2 nanoparticles may fall off from the film. For $TiO_2/Al(H_2PO_4)_3$ composite film, the solution can be analyzed without centrifugation, since TiO_2 nanoparticles were fixed on the framework of $Al(H_2PO_4)_3$. High-performance liquid chromatography (HPLC) was adopted to detect the intermediate products. HPLC condition: methyl cyanide and ammonium acetate (0.1 mol/L) as mobile phases (volume ratio: 40/60).

2.4. Evaluation of flushing resistance performance

The films were fixed at an angle of 30°. Then washing the films using DI water by a peristaltic pump at a flow velocity of 10 mL/min. The flushing time was 10 min. Then let the films air-dry and then dried at 60 °C for 30 min. The treated films were then used to evaluate the flushing resistance performance.

3. Results and discussion

3.1. Photocatalytic performance

Photocatalytic degradation of MB was adopted to evaluate the performance of different samples. As shown in Fig. 1a, the apparent rate constant of pure TiO_2 film was 5.63×10^{-3} min^{-1}. When introducing $Al(H_2PO_4)_3$ to the composite film, the apparent rate constant was promoted evidently. $TiO_2/Al(H_2PO_4)_3 - 0.2$ exhibited the highest photocatalytic activity and the apparent rate constant was approximately 7.94×10^{-3} min^{-1}, which is about 1.4-fold that of pure TiO_2 film. The enhanced performance may come from the less agglomeration of TiO_2 nanoparticles and the more exposed reactive sites. However, when the concentration of $Al(H_2PO_4)_3$ exceeded 0.4 g/L, the k value decreased slightly. The reason can be ascribed to the agglomeration of TiO_2 nanoparticles, which lead to the less exposed reactive sites. As is known, some intermediate products of MB in the process of photocatalytic reaction may be more toxic than MB itself. HPLC was adopted to detect whether the intermediate products of MB were degraded or not. As shown in Fig. 1b, the peaks at around 2.8 min represented MB and the peaks at around 2.4 min was intermediate products [13]. Both the peaks of MB and its intermediate products decreased as the reaction went on, which indicates that MB was mineralized completely rather than only converted into the intermediate. What is more, the peak intensity of MB and its intermediate products over $TiO_2/Al(H_2PO_4)_3$-0.2 composite film decreased more quickly than pure TiO_2 film.

In order to test the substrate selectivity of the composite film, glass slide was changed to metal mesh. As shown in Fig. 2a, degradation rule on metal mesh was almost the same as that on glass slide. $TiO_2/Al(H_2PO_4)_3 - 0.2$ exhibited the highest photocatalytic activity and the k value was approximately 3.30×10^{-2} min^{-1}, which is about 1.2-fold that of pure TiO_2 film. So, we can speculate that $TiO_2/Al(H_2PO_4)_3$ composite film has no selectivity towards different substrates, which is of vital importance in the field of self-clean. In order to investigate the solidity degree of this composite film, contrast test was carried on. As shown in Fig. 2b, after water flushing, the k value of pure TiO_2 film decrease about 84.0%, which can be ascribed to the loss of TiO_2 nanoparticles. However, the k value of $TiO_2/Al(H_2PO_4)_3 - 0.2$ composite film decrease only 31.7% and is 6.0-fold that of pure TiO_2 film, indicating that the composite film bears good washing resistance thanks to the good adhesive force of $Al(H_2PO_4)_3$ towards the substrate. More than that, the composite is separation-free and can be reused without further treatment.

3.2. Morphology and structural information

Scanning electron microscope (SEM) was adopted to investigate the cross-sectional view of the $TiO_2/Al(H_2PO_4)_3$-0.2 composite film. As shown in Fig. 3a, there was distinct interface between glass slide and the composite film and the sickness of the composite film was approximately 2–3 um. High resolution transmission electron microscopy (HRTEM) image of $TiO_2/Al(H_2PO_4)_3 - 0.2$ (shown in Fig. 3b and Fig. S2) exhibited clear lattice fringes of TiO_2 (d = 0.324 nm corresponds to rutile (110) crystal face, d = 0.218 nm corresponding to rutile (111) crystal face; d = 0.352 nm corresponds to anatase (101) crystal face, d = 0.189 nm corresponding to anatase (200) crystal face). Outside the TiO_2 nanoparticles were $Al(H_2PO_4)_3$, which is about 0.5–1.0 nm. The $Al(H_2PO_4)_3$ could prevent the agglomeration of TiO_2 nanoparticles and increase the reactive sites. To further investigate the distribution of $Al(H_2PO_4)_3$, EDS mapping analysis was carried on. As shown in Fig. 3f and 3 g, the elements of Al and P were distributed uniformly around the TiO_2 nanoparticles, demonstrating that $Al(H_2PO_4)_3$ was distributed uniformly.
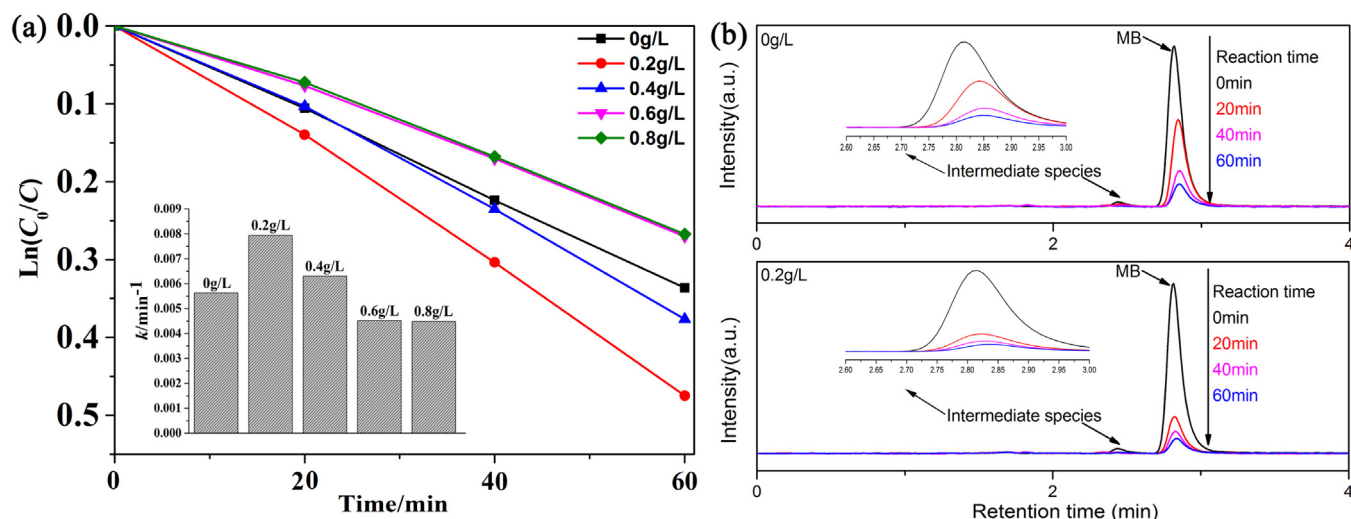
Fig. 1. (a) Photocatalytic performance of MB over $TiO_2/Al(H_2PO_4)_3$ composite film on glass slide under the irradiation of UV light ($\lambda = 254$ nm). (inset) the apparent rate constants: k. (b) HPLC intermediate product distribution of MB over $TiO_2/Al(H_2PO_4)_3$ composite film (0 g/L and 0.2 g/L).

Fig. S3a showed the UV–vis DRS spectra of different samples. As is shown, the absorption edge of TiO_2 located at 410 nm, while the absorption edge of $Al(H_2PO_4)_3$ located at 269 nm. $TiO_2/Al(H_2PO_4)_3$ exhibited almost the same absorption edge as pure TiO_2, indicating that the introducing of $Al(H_2PO_4)_3$ didn't change the energy band structure of TiO_2. The XRD patterns of different samples were shown in Fig. S3b. The diffraction peaks of TiO_2 fit well with JCPDS: 21-1272 (anatase, tetragonal) and JCPDS: 21-1276 (rutile, tetragonal) [34]. The diffraction peaks of $Al(H_2PO_4)_3$ correspond to JCPDS: 14-0546 (hexagonal). The diffraction peaks of $Al(H_2PO_4)_3$ could not be observed in $TiO_2/Al(H_2PO_4)_3$, indicating that $Al(H_2PO_4)_3$ existed in amorphous form. The XRD pattern of TiO_2 showed no change after modified by $Al(H_2PO_4)_3$, demonstrating that the introduction of $Al(H_2PO_4)_3$ did not change the crystal structure of TiO_2.

3.3. Origin of promoted performance

As is known, the photocatalytic performance was influenced by various factors, of which specific surface area and pore size are of vital importance. The specific surface area and pore size of different samples were shown in Table 1 and Fig. 4. The

Table 1
The specific surface area of different samples.

Sample	S_{BET} ($m^2\,g^{-1}$)
0 g/L	49.33
0.2 g/L	53.90
0.4 g/L	51.83
0.6 g/L	49.88
0.8 g/L	49.83
1 g/L	48.10

specific surface area of pure TiO_2 and $Al(H_2PO_4)_3$ was 49.33 and 48.10 $m^2\,g^{-1}$, respectively. Interestingly, the specific surface area of $TiO_2/Al(H_2PO_4)_3 - 0.2$ was the highest (53.90 $m^2\,g^{-1}$), indicating that a small amount of $Al(H_2PO_4)_3$ could prevent the agglomeration of TiO_2 nanoparticles and promote the specific surface area so as to increase the reactive sites and enhance the photocatalytic performance. However, when $Al(H_2PO_4)_3$ exceeded a certain amount, the specific surface area decreased, pore volume got larger (shown in Fig. 4) and the agglomeration of TiO_2 nanoparticles got more serious, resulting in the decline of photocatalytic activity (Fig. 1a).
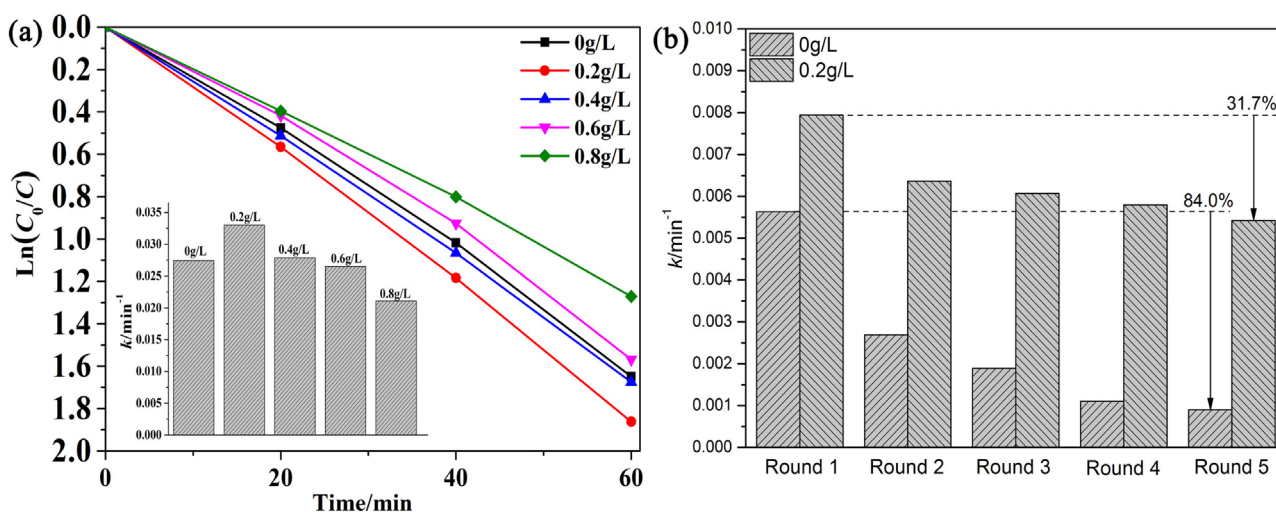
Fig. 2. (a) Photocatalytic performance of MB over $TiO_2/Al(H_2PO_4)_3$ composite film on metal mesh under the irradiation of UV light ($\lambda = 254$ nm). (inset) the apparent rate constants: k. (b) The apparent rate constants comparison after flushing over $TiO_2/Al(H_2PO_4)_3$ film (0 g/L and 0.2 g/L) on glass slide under the irradiation of UV light ($\lambda = 254$ nm).
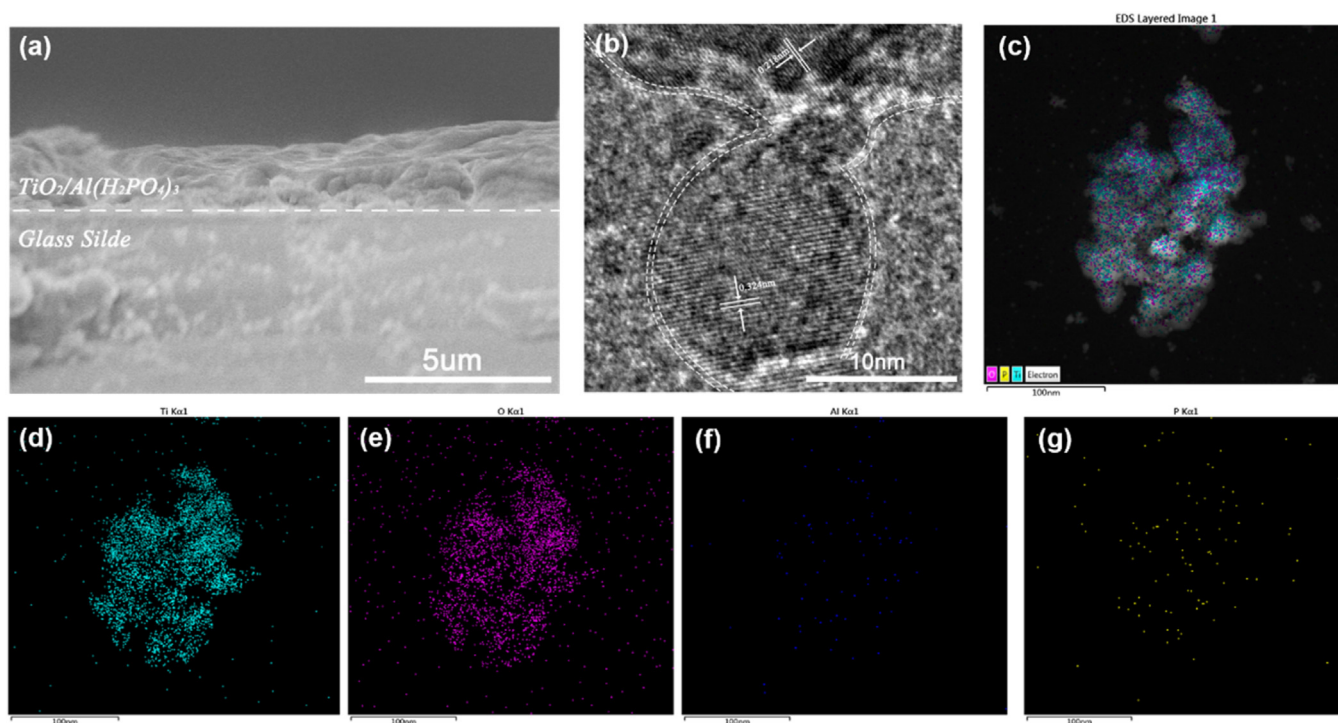
Fig. 3. (a) SEM images of the cross-sectional view (b) HRTEM image (c–g) EDS mapping images of $TiO_2/Al(H_2PO_4)_3$ composite film (0.2 g/L).

SEM images (Fig. S4) shows that the morphology of pure $Al(H_2PO_4)_3$ was bulk-shaped on the micron scale. The agglomeration of pure TiO_2 nanoparticles was relatively severe. When introducing $Al(H_2PO_4)_3$, the agglomeration of TiO_2 nanoparticles was prevented and no bulk $Al(H_2PO_4)_3$ was observed, which indicates that $Al(H_2PO_4)_3$ was dispersed on the surface of TiO_2 nanoparticles uniformly rather than mechanical mixing. That is why the diffraction peaks of $Al(H_2PO_4)_3$ could not be observed in $TiO_2/Al(H_2PO_4)_3$ (Fig. S3b). TEM was also adopted to observe the dispersibility of $TiO_2/Al(H_2PO_4)_3$. As shown in Fig. S5, the diameter of TiO_2 nanoparticles was around 50 nm and the agglomeration of pure TiO_2 nanoparticles was relatively serious. When introducing $Al(H_2PO_4)_3$, the agglomeration of TiO_2 nanoparticles was prevented. However, when the concentration of $Al(H_2PO_4)_3$ exceeded 0.4 g/L, the agglomeration got severe again, which is in accordance with the rule of photocatalytic performance (Fig. 1a) and specific surface area (Table 1).

Based on the above analysis, we can conclude that the introduction of a small amount of $Al(H_2PO_4)_3$ could prevent the agglomeration of TiO_2 nanoparticles and promote the specific

surface area so as to increase the reactive sites and enhance the photocatalytic performance. In order to explore the interaction between TiO_2 and $Al(H_2PO_4)_3$, Raman spectra were employed. In Fig. S6, TiO_2 showed major Raman peaks at 147, 403, 523 and 639 cm^{-1} [35]. The typical Raman bands originating from $Al(H_2PO_4)_3$ appeared at 923 and 1219 cm^{-1}, respectively [36]. Since the peak intensity of TiO_2 was much higher than that of $Al(H_2PO_4)_3$, the diffraction peaks of $Al(H_2PO_4)_3$ could not be observed in $TiO_2/Al(H_2PO_4)_3$. XPS was the most powerful tool to analyze the interaction between TiO_2 and $Al(H_2PO_4)_3$. As is expected (shown in Fig. 5a), O1s, Ti2p and P2p were observed in the XPS survey spectrum of $TiO_2/Al(H_2PO_4)_3$. It is interesting to note that the binding energy of both P2p and Ti2p in $TiO_2/Al(H_2PO_4)_3$ exhibited distinct shift compared with pure TiO_2 and $Al(H_2PO_4)_3$ (Fig. 5b and c), which indicates that there is some interaction between TiO_2 and $Al(H_2PO_4)_3$. The binding energy of P2p was shifted to lower binding energy. The lower binding energy indicates that P got electrons partially. Correspondingly, the binding energy of Ti2p was shifted to higher binding energy. The higher binding energy indicates that Ti lost electrons partially. So, we can conclude that there may be chemical bonds between TiO_2 and $Al(H_2PO_4)_3$, which results in the good adhesive force of $Al(H_2PO_4)_3$ and also contributed to the increased photocatalytic activity. The good adhesive force made the composite film separation-free and bear good washing resistance. To further confirm the chemical bonds between TiO_2 and $Al(H_2PO_4)_3$, we resolved the XPS peaks of P2p and Ti2p. As shown in Fig. 5b, no characteristic peak at 128.6 eV was observed, which indicates that there was no Ti—P bond in $TiO_2/Al(H_2PO_4)_3$ [37,38]. So, it was likely to form Ti—O—P bond between TiO_2 and $Al(H_2PO_4)_3$. The peak at 134.70 eV corresponds to the P in P—O bond while 133.72 eV corresponds to the P in Ti—O—P bond [39]. Similarly, as shown in Fig. 5c, the peaks at 464.33 eV ($Ti2p_{1/2}$) and 458.64 eV ($Ti2p_{3/2}$) correspond to the Ti in Ti—O bond while the peaks at 464.54 and 459.04 eV correspond to the Ti in Ti—O—P bond [39,40]. The spectrum of O1s in Fig. 5d could be resolved to three peaks at 532.72 eV, 531.05 eV and 529.89 eV, corresponding to the O in P—O—H or Al—O, Ti—O—P or P=O, and Ti—O, respectively [39]. Based on the above
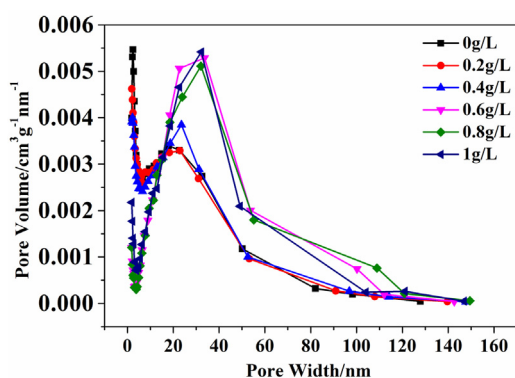

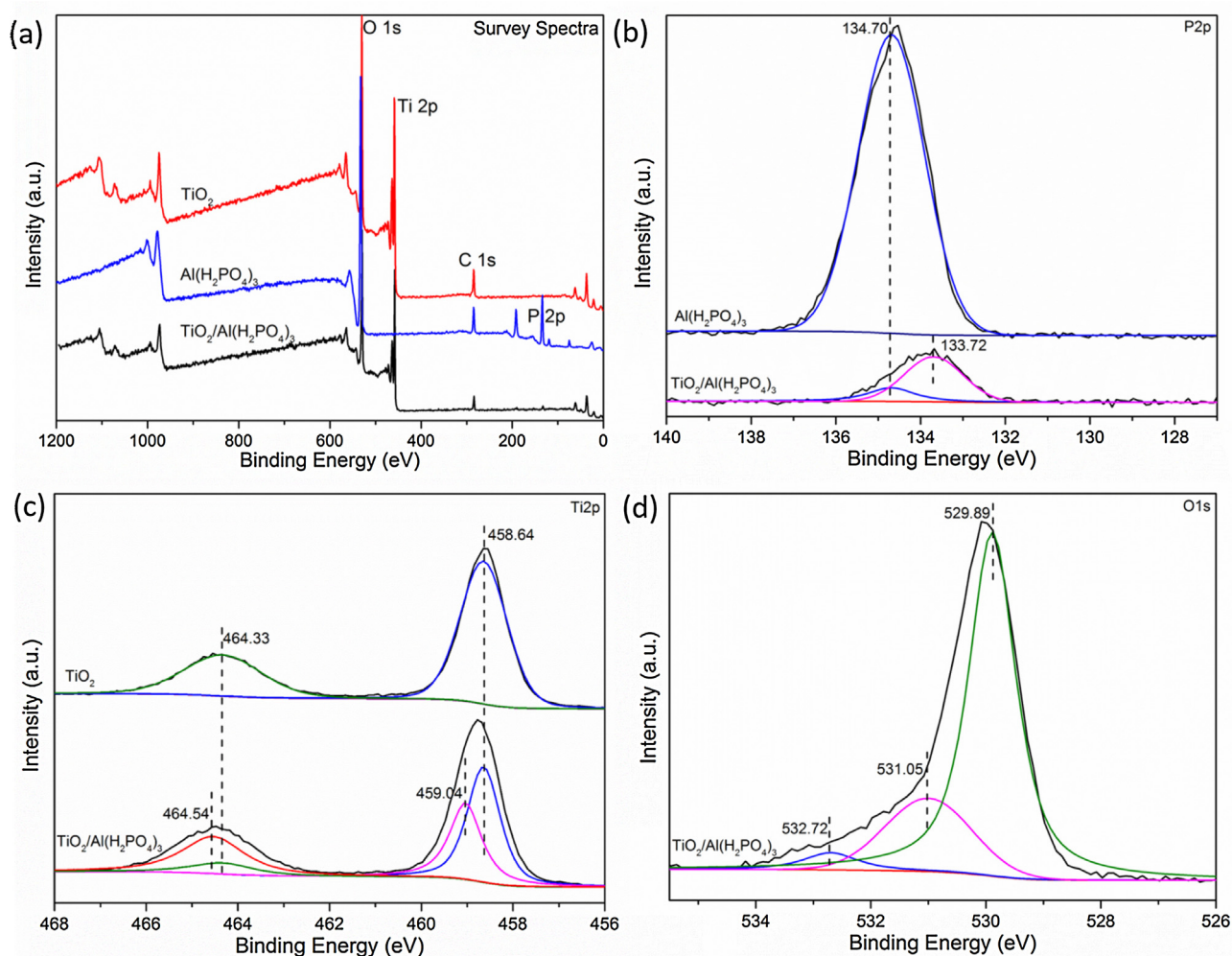Fig. 4. Pore size distribution of $TiO_2/Al(H_2PO_4)_3$ composite film.

Fig. 5. (a) XPS survey spectra of different samples. High-resolution XPS spectra of different samples: (b) P2p, (c) Ti2p and (d) O1s.

analysis, we can conclude that Ti—O—P bond was formed between TiO_2 and $Al(H_2PO_4)_3$. There were two routes to form Ti—O—P bond. One is that the O in TiO_2 combine with the P in $Al(H_2PO_4)_3$. Another is that the Ti in TiO_2 combine with the O—P in $Al(H_2PO_4)_3$. Usually, the chemical bonds formed between metallic elements and non-metallic elements were ionic bond and the chemical bonds formed between nonmetallic elements were covalent bond. So, the Ti—O in Ti—O—P bond could be assigned to ionic bond while the O—P in Ti—O—P bond could be assigned to covalent bond.

In order to explore the main oxidative species in the system, trapping experiments were tested. t-BuOH was acted as hydroxyl radical scavenger [41], EDTA-2Na was acted as scavenger of holes [42]. Blank test in Fig. 6 indicates that MB showed slight self-degradation under UV light. Hydroxyl radical inhibited the photocatalytic activity slightly. However, hole scavenger inhibited the photocatalytic activity distinctly, which demonstrates that holes were the dominant oxidative species.

Based on the above analysis, a feasible mechanism of the enhanced photocatalytic performance was put forward. As shown in Fig. 7, TiO_2 nanoparticles were dispersed uniformly on the surface of the glass slide thanks to the good adhesive force of $Al(H_2PO_4)_3$, which could prevent the agglomeration of TiO_2 nanoparticles and promote the specific surface area so as to increase the reactive sites and enhance the photocatalytic performance. Under UV light, electrons were excited from the VB to the CB of TiO_2 [43]. Holes could oxidize organic pollutants directly [44].

Meanwhile, the electrons could combine with O_2 to form $O_2{}^{\bullet-}$, which could partake in the degradation of the organic pollutants [45]. On the other hand, TiO_2 nanoparticles were fixed on the framework of $Al(H_2PO_4)_3$, making the composite film separation-free and bear good washing resistance.

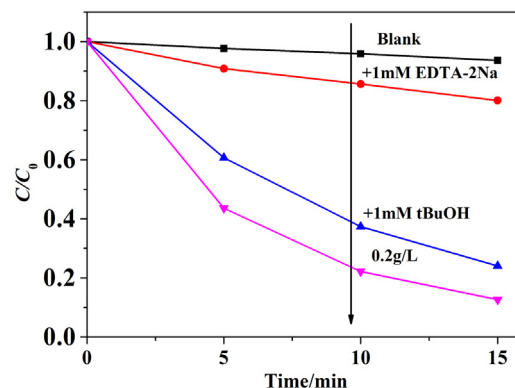**Fig. 6.** Photogenerated carriers trapping test over $TiO_2/Al(H_2PO_4)_3$ composite film (0.2 g/L) under UV light.

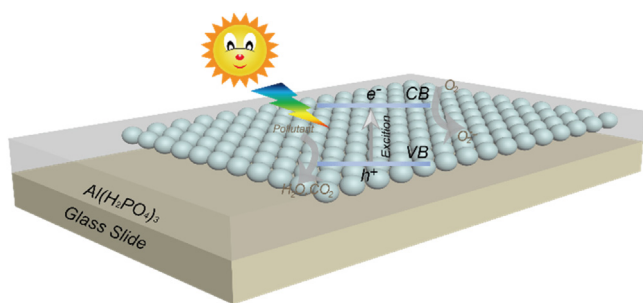**Fig. 7.** Schematic diagram of the enhanced photocatalytic performance.

4. Conclusion

In this work, $TiO_2/Al(H_2PO_4)_3$ composite film was constructed via a facile spray method. The composite film exhibited higher photocatalytic activity compared with pure TiO_2. TiO_2 nanoparticles were dispersed uniformly on the surface of the glass slide, which could prevent the agglomeration of TiO_2 nanoparticles and increase the reactive sites. More importantly, TiO_2 nanoparticles were fixed on the framework of $Al(H_2PO_4)_3$, making the composite film separation-free and bear good washing resistance thanks to the good adhesive force of $Al(H_2PO_4)_3$. The good adhesive force could be ascribed to the formation of Ti—O—P bond between TiO_2 and $Al(H_2PO_4)_3$, which also contributed to the increased photocatalytic activity. This work presents a feasible method of fabricating TiO_2-based separation-free and washing-resistance film, which may hold potential applications in the field of self-clean.

Acknowledgements

Appendix A. Supplementary data

Supplementary data associated with this article can be found, in the online version, at http://dx.doi.org/10.1016/j.apcatb.2016.11.026.

References

[1] H. Park, H. Kim, G. Moon, W. Choi, Energ. Environ. Sci. 9 (2015) 411–433.
[2] X. Li, J. Yu, M. Jaroniec, Chem. Soc. Rev. 45 (2016) 2603–2636.
[3] H. Tong, S. Ouyang, Y. Bi, N. Umezawa, M. Oshikiri, J. Ye, Adv. Mater. 24 (2012) 229–251.
[4] A. Iwase, Y.H. Ng, Y. Ishiguro, A. Kudo, R. Amal, J. Am. Chem. Soc. 133 (2011) 11054–11057.
[5] Y. Huang, S. Kang, Y. Yang, H. Qin, Z. Ni, S. Yang, X. Li, Appl. Catal. B: Environ. 196 (2016) 89–99.
[6] C. Pan, Y. Zhu, Catal. Sci. Technol. 5 (2015) 3071–3083.
[7] L. Zhang, Y. Zhu, Catal. Sci. Technol. 2 (2012) 694–706.
[8] J. Sheng, X. Li, Y. Xu, ACS Catal. 4 (2014) 732–737.
[9] W. Jiang, Y. Liu, R. Zong, Z. Li, W. Yao, Y. Zhu, J. Mater. Chem. A 3 (2015) 18406–18412.
[10] J. Zhang, L. Qi, J. Ran, J. Yu, S.Z. Qiao, Adv. Energy Mater. 4 (2014) 1301925.
[11] J. Zhang, J. Yu, M. Jaroniec, J.R. Gong, Nano Lett. 12 (2012) 4584–4589.
[12] Q. Li, X. Li, S. Wageh, A. Al-Ghamdi, J. Yu, Adv. Energy Mater. 5 (2015) 1500010.
[13] W. Jiang, W. Luo, R. Zong, W. Yao, Z. Li, Y. Zhu, Small 12 (2016) 4370–4378.
[14] W. Jiang, W. Luo, J. Wang, M. Zhang, Y. Zhu, J. Photochem. Photobiol. C 28 (2016) 87–115.
[15] Y. Zheng, L. Lin, B. Wang, X. Wang, Angew. Chem. Int. Ed. 54 (2015) 12868–12884.
[16] W. Jiang, Y. Liu, J. Wang, M. Zhang, W. Luo, Y. Zhu, Adv. Mater. Interfaces 3 (2016) 1500502 http://dx.doi.org/10.1002/admi.201500502.
[17] Z. Bian, J. Zhu, H. Li, J. Photochem. Photobiol. C 28 (2016) 72–86.
[18] Z. Li, J. Sheng, Y. Zhang, X. Li, Y. Xu, Appl. Catal. B: Environ. 166–167 (2015) 313–319.
[19] B. Cao, G. Li, H. Li, Appl. Catal. B: Environ. 194 (2016) 42–49.
[20] T. Kamegawa, Y. Ishiguro, H. Seto, H. Yamashita, J. Mater. Chem. A 3 (2015) 2323–2330.
[21] J. Zhu, J. Wang, F. Lv, S. Xiao, C. Nuckolls, H. Li, J. Am. Chem. Soc. 135 (2013) 4719–4721.
[22] Z. Chen, D. Zhang, X. Wang, X. Jia, F. Wei, H. Li, Y. Lu, Adv. Mater. 24 (2012) 2030–2036.
[23] L. Zhang, W. Wang, L. Zhou, M. Shang, S. Sun, Appl. Catal. B: Environ. 90 (2009) 458–462.
[24] T. Cheng, D. Zhang, H. Li, G. Liu, Green Chem. 16 (2014) 3401–3427.
[25] M. Shang, W. Wang, J. Ren, S. Sun, L. Wang, L. Zhang, J. Mater. Chem. 19 (2009) 6213–6218.
[26] J.-G. Yu, H.-G. Yu, B. Cheng, X.-J. Zhao, J.C. Yu, W.-K. Ho, J. Phys. Chem. B 107 (2003) 13871–13879.
[27] M. Wilkinson, A. Kafizas, S.M. Bawaked, A.Y. Obaid, S.A. Al-Thabaiti, S.N. Basahel, C.J. Carmalt, I.P. Parkin, ACS Comb. Sci. 15 (2013) 309–319.
[28] M.J. Powell, R. Quesada-Cabrera, A. Taylor, D. Teixeira, I. Papakonstantinou, R.G. Palgrave, G. Sankar, I.P. Parkin, Chem. Mater. 28 (2016) 1369–1376.
[29] T. Frade, V. Bouzon, A. Gomes, M.I. da Silva Pereira, Surf. Coat. Technol. 204 (2010) 3592–3598.
[30] M. Pelaez, P. Falaras, V. Likodimos, A.G. Kontos, A.A. de la Cruz, K. O'Shea, D.D. Dionysiou, Appl. Catal. B: Environ. 99 (2010) 378–387.
[31] T. Fu, Y. Shen, Z. Alajmi, S. Yang, J. Sun, H. Zhang, Mater. Sci. Technol.-Lond. 31 (2015) 501–505.
[32] M. Mazur, D. Wojcieszak, J. Domaradzki, D. Kaczmarek, S. Song, F. Placido, Opt.-Electron. Rev. 21 (2013) 233–238.
[33] H.-J. Han, D.-P. Kim, J. Sol-Gel Sci. Technol. 26 (2003) 223–228.
[34] G. Zhou, R. Dou, H. Bi, S. Xie, Y. Pei, K. Fan, M. Qiao, B. Sun, B. Zong, J. Catal. 332 (2015) 119–126.
[35] X. Yang, J. Qin, Y. Jiang, K. Chen, X. Yan, D. Zhang, R. Li, H. Tang, Appl. Catal. B: Environ. 166 (2015) 231–240.
[36] B. Ravikumar, R. Rajaram, V. Ramakrishnan, J. Raman Spectrosc. 37 (2006) 597–605.
[37] J.-Y. Luo, L.-J. Chen, Y.-J. Zhao, P. He, Y.-Y. Xia, J. Power Sources 194 (2009) 1075–1080.
[38] S. Baunack, S. Oswald, D. Scharnweber, Surf. Interface Anal. 26 (1998) 471–479.
[39] H. Fei, X. Zhou, H. Zhou, Z. Shen, P. Sun, Z. Yuan, T. Chen, Microporous Mesoporous Mater. 100 (2007) 139–145.
[40] C.P. Sajan, S. Wageh, A.A. Al-Ghamdi, J. Yu, S. Cao, Nano Res. 9 (2016) 3–27.
[41] G. Dong, W. Ho, L. Zhang, Appl. Catal. B: Environ. 168 (2015) 490–496.
[42] L. Yang, Z. Li, H. Jiang, W. Jiang, R. Su, S. Luo, Y. Luo, Appl. Catal. B: Environ. 183 (2016) 75–85.
[43] W. Li, D. Li, J. Wang, Y. Shao, J. You, F. Teng, J. Mol. Catal. A: Chem. 380 (2013) 10–17.
[44] K. Li, S. Gao, Q. Wang, H. Xu, Z. Wang, B. Huang, Y. Dai, J. Lu, ACS Appl. Mater. Interfaces 7 (2015) 9023–9030.
[45] B. Qiu, Y. Zhou, Y. Ma, X. Yang, W. Sheng, M. Xing, J. Zhang, Sci. Rep. 5 (2015).